Journal of
Instrumentation

Ultra-high precision high voltage system for PTOLEMY

Published by IOP Publishing for Sissa Medialab

Received: *December 31, 2025*
Accepted: *March 8, 2026*
Published: *April 15, 2026*

Ultra-high precision high voltage system for PTOLEMY

The PTOLEMY collaboration

R. Ammendola,[a] **A. Apponi,**[b] **G. Benato,**[c,d] **M.G. Betti,**[e,f] **R. Biondi,**[c,d] **P. Bos,**[g,h] **G. Cavoto,**[e,f] **M. Cadeddu,**[i] **A. Casale,**[k] **O. Castellano,**[b,ad] **E. Celasco,**[l,m] **L. Cecchini,**[e] **M. Chirico,**[e,f] **W. Chung,**[n] **A.G. Cocco,**[c] **A.P. Colijn,**[g,h] **B. Corcione,**[e,f] **N. D'Ambrosio,**[c] **M. D'Incecco,**[c] **G. De Bellis,**[e,ae] **M. De Deo,**[c] **N. de Groot,**[p] **A. Esposito,**[e,f] **M. Farino,**[n] **S. Farinon,**[m] **A.D. Ferella,**[c,o] **L. Ferro,**[i,j] **L. Ficcadenti,**[e] **G. Galbato Muscio,**[e,ae] **S. Gariazzo,**[q,r,ab] **H. Garrone,**[q,s,t] **F. Gatti,**[l,m] **G. Korga,**[aa] **F. Malnati,**[q,s,af] **G. Mangano,**[u,v] **L.E. Marcucci,**[w,x] **C. Mariani,**[e,f] **J. Mead,**[g,h] **G. Menichetti,**[x] **M. Messina,**[c] **E. Monticone,**[q,s] **M. Naafs,**[g] **V. Narcisi,**[a,ac] **S. Nagorny,**[c,d] **G. Neri,**[l,m] **F. Pandolfi,**[e] **R. Pavarani,**[i,j] **C. Pérez de los Heros,**[z] **O. Pisanti,**[u,v] **C. Pepe,**[s,1] **F.M. Pofi,**[c,d] **A.D. Polosa,**[e,f] **I. Rago,**[e] **M. Rajteri,**[q,s] **N. Rossi**,[c,*] **S. Ritarossi,**[b,ad] **A. Ruocco,**[b,ad] **G. Salina,**[a] **A. Santucci,**[i,j,ac] **M. Sestu,**[i,j] **A. Tan,**[n] **V. Tozzini,**[w,y] **C.G. Tully,**[n,*] **I. van Rens,**[p] **F. Virzi,**[c,o] **G. Visser**[g] **and M. Viviani**[x]

[a] *INFN Sezione di Roma Tor Vergata, Roma, Italy*
[b] *INFN Sezione di Roma Tre, Roma, Italy*
[c] *INFN Laboratori Nazionali del Gran Sasso (LNGS), L'Aquila, Italy*
[d] *Gran Sasso Science Institute (GSSI), L'Aquila, Italy*
[e] *INFN Sezione di Roma, Roma, Italy*
[f] *Dipartimento di Fisica, Sapienza Università di Roma, Roma, Italy*
[g] *Nationaal instituut voor subatomaire fysica (NIKHEF), Amsterdam, The Netherlands*
[h] *Department of Physics, University of Amsterdam, Amsterdam, The Netherlands*
[i] *INFN Sezione di Cagliari, Cagliari, Italy*
[j] *Dipartimento di Fisica, Università di Cagliari, Cagliari, Italy*
[k] *Department of Physics, Columbia University, New York, U.S.A.*
[l] *INFN Sezione di Genova, Genova, Italy*
[m] *Dipartimento di Fisica, Università di Genova, Genova, Italy*
[n] *Department of Phsysics, Princeton University, Princeton NJ, U.S.A.*
[o] *Dipartimento di Fisica, Università degli Studi dell'Aquila, L'Aquila, Italy*
[p] *Department of Physics, Radboud University, Nijmegen, The Netherlands*
[q] *INFN Sezione di Torino, Torino, Italy*
[r] *Dipartimento di Fisica, Università di Torino, Torino, Italy*

[*] Corresponding author.
[1] Now at CSIC — Institut de Microelectrònica de Barcelona (IMB-CNM).

https://doi.org/10.1088/1748-0221/21/04/P04009

[s] Istituto Nazionale di Ricerca Metrologica (INRiM), Torino, Italy
[t] Dipartimento di Elettronica & Telecomunicazioni (POLITO-ELN), Politecnico di Torino, Torino, Italy
[u] INFN Sezione di Napoli, Napoli, Italy
[v] Dipartimento di Fisica, Università degli Studi di Napoli Federico II, Napoli, Italy
[w] INFN Sezione di Pisa, Pisa, Italy
[x] Dipartimento di Fisica, Università di Pisa, Pisa, Italy
[y] CNR-Instituto Nanoscienze, Pisa, Italy
[z] Department of Physics and Astronomy, Uppsala University, Uppsala, Sweden
[aa] Department of Physics, University of Oxford, Oxford, U.K.
[ab] Instituto de Fisica Corpuscular (IFIC — CSIC/UV), Paterna (Valencia), Spain
[ac] Agenzia nazionale per le nuove tecnologie, l'energia e lo sviluppo economico sostenibile (ENEA), Frascati (Roma), Italy
[ad] Dipartimento di Scienze, Università degli Studi di Roma Tre, Roma, Italy
[ae] Dipartimento di Ingegneria Astronautica, Elettrica ed Energetica, Sapienza Università di Roma, Roma, Italy
[af] Dipartimento Scienza Applicata e Tecnologia, Politecnico di Torino, Torino, Italy

E-mail: nicola.rossi@lngs.infn.it, cgtully@princeton.edu

Abstract: The PTOLEMY project is prototyping a novel electromagnetic filter for high-precision β spectroscopy, with the ultimate and ambitious long-term goal of detecting the cosmic neutrino background through electron capture on tritium bound to graphene. Intermediate small-scale prototypes can achieve competitive sensitivity to the effective neutrino mass, even with reduced energy resolution. To reach an energy resolution better than 500 meV at the tritium β-spectrum endpoint of 18.6 keV, and accounting for all uncertainties in the filtering chain, the electrode voltage must be controlled at the level of a few parts per million and monitored in real time. In this work, we present the first results obtained in this effort, using a chain of commercial ultra-high-precision voltage references, read out by precision multimeters and a *field mill* device. The currently available precision on high voltage is, in the conservative case, as low as 0.2 ppm per 1 kV single board and $\lesssim$ 50 mV over the 10 kV series, presently limited by field mill read-out noise. However, assuming uncorrelated Gaussian noise extrapolation, the real precision could in principle be as low as 0.05 ppm over 20 kV.

Keywords: Neutrino detectors; Digital signal processing (DSP); Modular electronics; Analysis and statistical methods

ArXiv ePrint: 2512.19437

2026 JINST 21 P04009

Contents

Introduction

The detection of the cosmic neutrino background (CνB), decoupled just one second after the Big Bang initial singularity, would provide a unique opportunity to test the standard cosmological model in the very early Universe [1, 2]. Although the CνB is the most abundant source of neutrinos in the Universe, its detection is extremely challenging due to the very low energy of these so-called relic neutrinos. One of the most promising detection channels to overcome this difficulty is the decay of β-unstable elements induced by their interaction with the CνB [3]. When a CνB neutrino interacts with a β-unstable isotope, it results in the emission of a monochromatic electron, shifted from the β-spectrum end-point by an energy interval equal to twice the effective neutrino mass. Consequently, any attempt to detect CνB features inherently requires extremely high sensitivity to the effective neutrino mass, a key missing parameter of the Standard Model that has yet to be experimentally determined. The current best limit in this direction has been set by the KATRIN Collaboration, which reports $m_{\nu_e}^{\text{eff}} < 450\,\text{meV}$ (90% CL) with an energy resolution of approximately 1 eV on the β-spectrum [4].

The PTOLEMY project is exploring the use of tritium atoms (^{3}H) bound to graphene layers (*tritiated graphene*) to enhance both the stability and efficiency of the target [5, 6]. Based on indirect constraints [7], the expected effective neutrino mass is likely below 200 meV, requiring extremely high energy resolution for CνB detection. However, for effective neutrino mass measurement, a comparatively lower resolution of $\lesssim 500\,\text{meV}$ would still be competitive with the current generation experiments [2]. To achieve this goal, the PTOLEMY Collaboration is proposing a novel electromagnetic filter composed of multiple modules, each of which must contribute minimally to the overall energy resolution. In particular, the high-voltage (HV) electrodes must maintain accuracy within a few parts per million (ppm) over about 20 kV.

The aim of this work is to describe the HV control and stabilization approach investigated by the Collaboration and to present the first direct measurements. In section 1, a detailed description of the PTOLEMY demonstrator and its modules is provided. In section 2, the HV stability system adopted by the Collaboration is thoroughly discussed. Finally, in section 3, the first results on HV stability are presented and analyzed.

2026 JINST 21 P04009

1 The PTOLEMY Demonstrator

The goal of the PTOLEMY Demonstrator, which is being built at Laboratori Nazionali del Gran Sasso (INFN) [8], is to prove the viability of the PTOLEMY detection concept [5, 6] on a reduced scale, exploring the criticalities of its individual modules both separately and in combination. Once all technical aspects are assessed, the Demonstrator can be rearranged for a real experiment to explore the neutrino mass with a small target of $1 \div 100\,\mu g$ of tritium, preliminarily addressed in [2]. As schematically depicted in the flow chart reported in figure 1, the PTOLEMY concept consists of the following four modules.

(i) *Tritiated graphene target:* tritium, featuring a low Q-value (18.6 eV), useful half-life (12.3 y), simple nuclear structure, and a relatively high cross section for neutrino capture (3.8×10^{-45} cm^2), is one of the best candidates for the physics investigated by PTOLEMY. It is possible to load it onto a graphene layer with high efficiency and stability [9, 10].

(ii) *Cyclotron radiation emission spectroscopy (CRES):* electrons from the tritium β decay are directed into a region with a high constant magnetic field (1 T) and a suitable electric field allowing for bouncing and $\mathbf{E}\times\mathbf{B}$ drift (*RF tracker*) [14]. The radio-frequency (RF) emission associated with the cyclotron motion is detected by an RF antenna, exploiting a technology similar to the one used in Project-8 [11, 15]. The detected RF provides information about the energy and transverse momentum of the electron.

(iii) *Dynamic electromagnetic filter:* if the RF detection indicates that the electron has an energy reasonably close to the Q-value, a *fast switch* within $\simeq$ 1 ms tunes the HV in order to allow the electron to pass through the filter. Unlike KATRIN, which transforms transverse momentum into parallel momentum over a gigantic volume, the constant drift filter requires a region of the order of a meter. This region is characterized by non uniform and mutually perpendicular magnetic and electric fields, allowing $\mathbf{E}\times\mathbf{B}$ and $\mathbf{B}\times\nabla B$ magnetic drifts to convert kinetic energy into potential one, see details in [12, 13].

(iv) *Final electron detection:* the energy of the selected electron, slowed down to a few hundreds of eV, is eventually measured in a high-precision calorimetric system. At the moment the Collaboration is considering two options: (a) microcalorimeters based on titanium-based transition-edge sensors (TES) [16] and (b) hemispherical electron energy analyzers [17].

As shown in figure 1, the total energy of the selected electron is given by the different contributions of each module acting on the traveling particle from the source to the high-precision calorimeters. The total uncertainty, $\sigma_{\rm TOT}$, of the electron energy required for high-precision β-spectroscopy is conceptually given by the combinations of the most important sources of uncertainties (either statistical, systematic, or related to any possible change of efficiency),

$$\sigma_{\rm TOT} \approx \sigma_{\rm Source} \otimes \sigma_{\rm RF} \otimes \sigma_{\rm Filter} \otimes \sigma_{\rm Det}\,, \tag{1.1}$$

where $\sigma_{\rm Source}$ represents the condensed-matter model uncertainty of electrons bound on graphene [18, 19], $\sigma_{\rm RF}$ accounts for energy loss due to RF emission (quantifiable as $\sim 7\,{\rm meV}/\mu{\rm s}$), $\sigma_{\rm Filter}$ is primarily related to the HV applied to the filter electrodes, and $\sigma_{\rm Det}$ corresponds to the energy resolution of the final high-precision calorimeter. The symbol $\otimes$ reduces to the sum in quadratures in case those quantities are uncorrelated.

2026 JINST 21 P04009

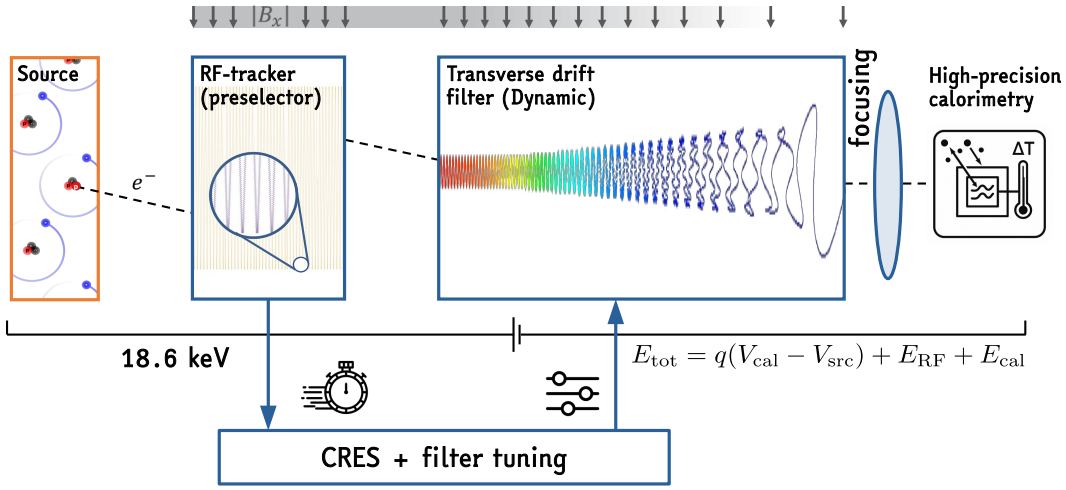

Figure 1. Schematic of the PTOLEMY concept. From left to right: tritiated graphene target, RF detection antenna (CRES) and fast trigger, dynamic electromagnetic filter and high-precision calorimeter.

The next section describes in detail the strategy adopted by the PTOLEMY Collaboration to minimize the uncertainty in the HV of the filter electrode, hereafter denoted by $\sigma_{\rm HV}$. It is indeed assumed that the systematic uncertainty associated with the filter is basically dominated by the uncertainty in the HV (i.e. $\sigma_{\rm Filter} \simeq \sigma_{\rm HV}$).

2 The precision HV system

The precision of the HV, denoted as $\sigma_{\rm HV}$, is directly related to the uncertainty in the voltage, given by

$$\sigma_{\rm HV} \simeq \frac{\delta V}{V} E_{\rm e}, \tag{2.1}$$

where V is the total voltage applied to slow down the electron to a few hundreds of eV, δV is its uncertainty and $E_{\rm e}$ is the β emission energy. Since the tritium end-point is at 18.6 keV, the total applied voltage should be on the order of 20 kV. From the simple relation in eq. (2.1), achieving the challenging energy resolution of 50 meV requires $\delta V/V \lesssim 2.5$ ppm.

Before proceeding further, it is important to clarify that two aspects must be carefully controlled in the voltage reference: both *precision* and *accuracy*. The first refers to the consistency of measurements under unchanged conditions, while the second relates to the proximity of measurement results to the accepted value. In the following, both of these crucial aspects will be discussed. Moreover, the precision, in this sense, is the sum in quadrature of two contributions: the local fluctuations, which must be averaged, and a possible long-term component. The latter is more properly referred to as *stability*. When comparing with other experiments, these two terms may have different meanings depending on the context. For example, in the KATRIN experiment, due to the integral spectrum measurement, the stability is particularly important. In contrast, in PTOLEMY, which performs a differential spectrum measurement, long-term drifts do not significantly affect the final result, as they

2026 JINST 21 P04009

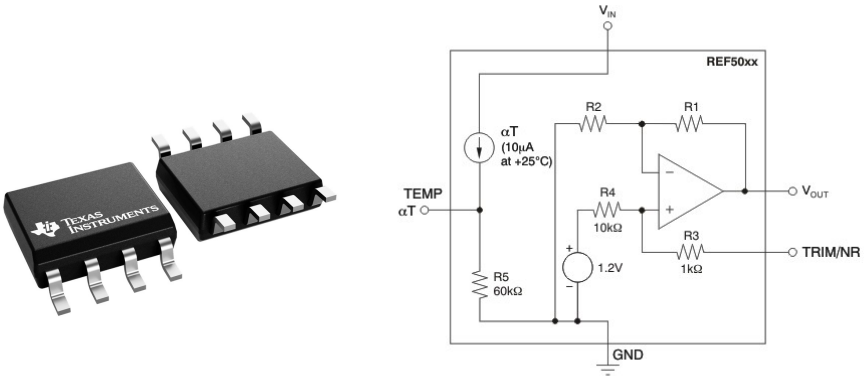

Figure 2. REF5010 ultra-high precision voltage reference by *Texas Instruments*. *Left:* visual appearance of the electronic component. *Right:* corresponding circuit diagram.

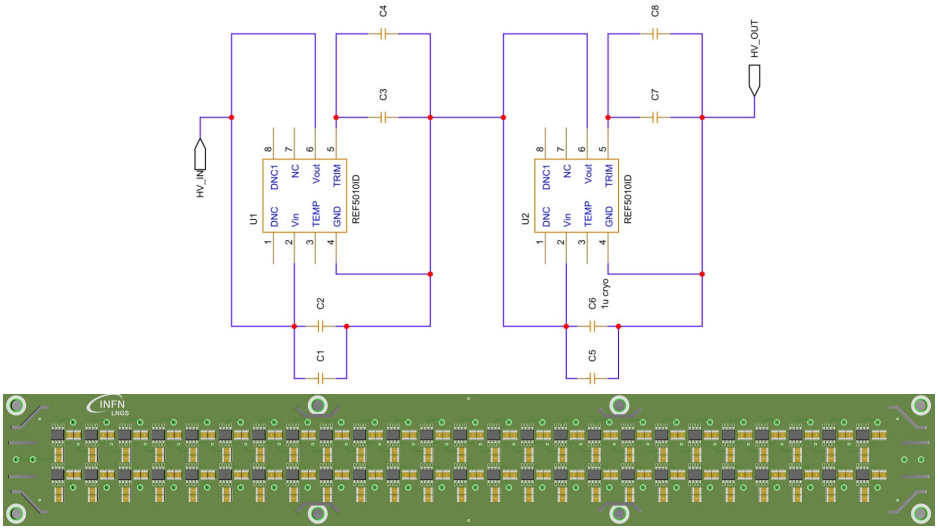

Figure 3. Schematic of the repeated chain module (*top*) developed at LNGS electronics laboratory. Drawing of the 1 kV board (*bottom*).

can be accounted for in the total energy uncertainty in eq. (1.1). However, a slow drift in the reference voltage could in principle mildly affect the filter efficiency, and this effect is under investigation by the Collaboration through a detailed filter simulation.

The strategy adopted by the Collaboration relies on an *ultra-high precision* voltage reference chain (or stack) [20] and its readout, consisting of a *precision multimeter* (for voltages lower than 1 kV, essential for ensuring accuracy) and a *field mill* non-invasive online monitoring system (for the full 20 kV voltage, enabling final precision).

The basic concept behind the voltage reference chain is that, even if the single component of the voltage reference chain has a limited precision, combining a number N of them under the hypothesis of Gaussian (σ) and uncorrelated noise, one can reach an ultra-high precision of the order $\sigma/\sqrt{N}$. In fact, the authors of [20] report a precision of $5 \div 7$ ppm over 1 kV after long testings. To a similar

2026 JINST 21 P04009

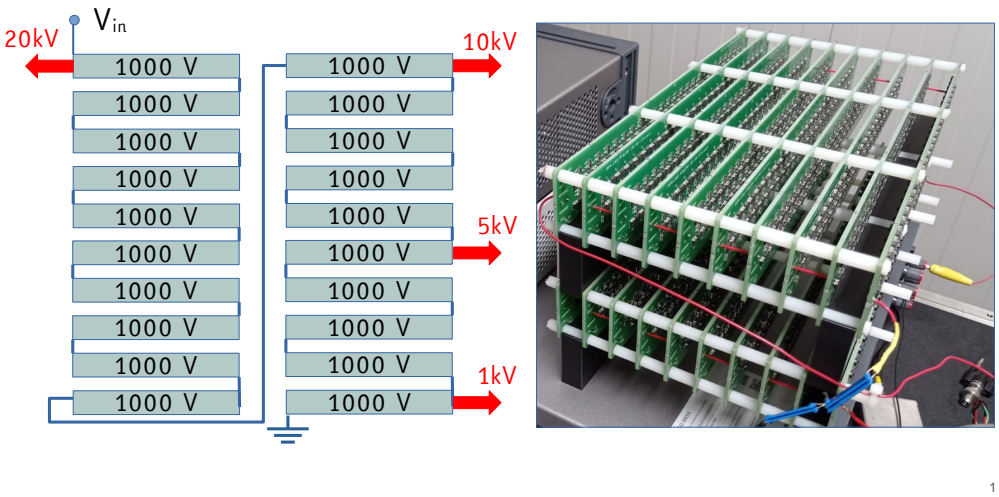

Figure 4. REF Chain. *Left:* schematic of the REF chain showing V_{in} with the four *slow switch* pins. *Right:* visual appearance of the twenty 1 kV boards, arranged in two layers, as operated at LNGS during tests.

purpose, the KATRIN Collaboration has instead developed a high voltage divider, consisting of high precision resistors kept at constant and stable temperature and read out by a high precision multimeter [21], reaching a comparable precision. Nonetheless, after preliminary investigations, the PTOLEMY Collaboration decided to pursue the voltage reference chain testings, as they show a large profit margin, as will be discussed in this article.

The basic unit of the HV system is a high precision voltage reference, REF5010 (hereafter REF), produced by *Texas Instruments* [22]. Figure 2 shows the visual appearance of the electronic component (*left*) and its corresponding circuit diagram (*right*). According to the data-sheet provided by the manufacturer, each REF accepts an input voltage of $V_{\text{in}} = 10.2 \div 18$ V, returning a nominal stable output of $V_{\text{out}} = 10$ V with a quiescent current of $I_{\text{q}} = 0.8$ mA. Furthermore, the temperature drift is extremely low (2.5 ppm/ °C), and accuracy is guaranteed at the level of 0.05% (high grade) per component. The intrinsic noise is reported as 0.5 µVpp/V. Finally, each REF features excellent long-term stability over time: 22 ppm/1000 h and operates over a wide temperature range of $-40 \div 125$ °C.

As shown in figures 3 and 4, the 10 V REFs are arranged in series to form a long chain composed of 20 boards of 1 kV each, summing up to 20 kV. The boards are designed and customized in the electronics workshop of the *Gran Sasso National Laboratories* (LNGS) according to the schematic depicted in figure 3. In particular, the final version, showing improved performance, was developed after extensive testing of the electronic components.

The choice of the plastic capacitor Panasonic ECPU1C105MA5 made it possible to reduce the noise to one third compared to a ceramic capacitor with X7R dielectric; TransZorb surge suppressors (transient voltage suppression diodes designed to protect against voltage spikes) were also added for safety reasons, and the routing is HV type, designed with proper insulation clearances and including milling slots to increase isolation at critical points.

The full chain is finally powered by a high-voltage Bertan 210-30R power supply. Along the chain, thanks to a *slow switch* mechanical device operated by a microcontroller-driven actuator,

2026 JINST 21 P04009

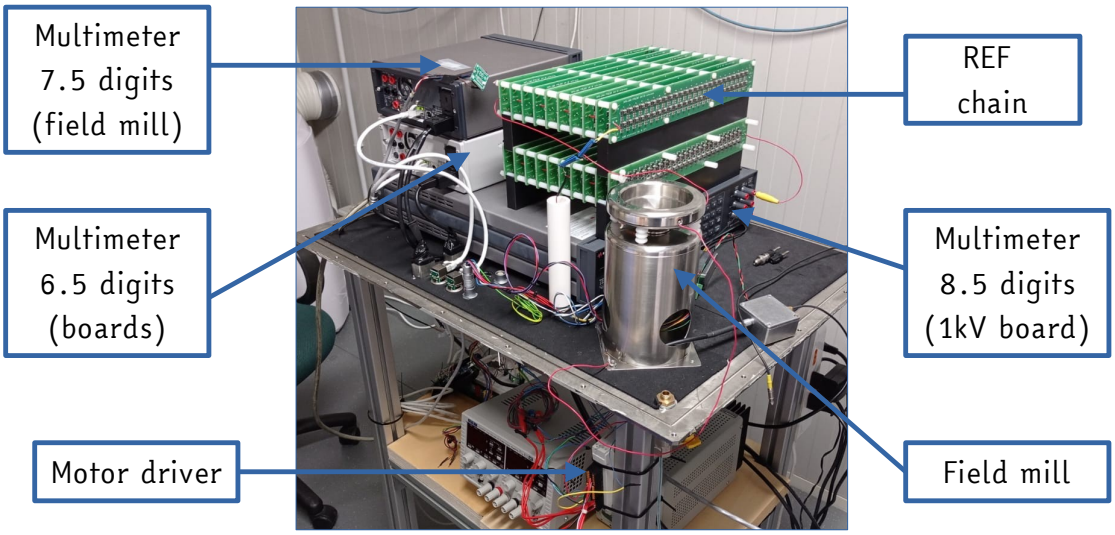

Figure 5. Bench test of the HV system. According to the descriptions in the picture, the REF chain is monitored by an $8^1/_2$-digit precision multimeter (for the 1 kV board only) and by the *field mill*, read out by a $7^1/_2$-digit precision multimeter, according to the *slow switch configuration*. Finally, the board temperature is read out by a 6.5-digit precision multimeter.

it is possible to switch in real-time between four different voltages (namely 1, 5, 10, and 20 kV) without physically altering the system.

The REF board chain is installed on a test bench and connected to the readout system as illustrated in figure 5. Single boards of 1 kV REFs can be monitored by an $8^1/_2$-digit precision multimeter Keysight 3458A up tp 1 kV corresponding to the full-scale of the device. The *field mill* (see description below) accepts higher voltages up to 20 kV according to the *slow switch* configuration, and its periodic voltage signal is read out by a $7^1/_2$-digit precision multimeter Keysight 34470A. Finally, a third $6^1/_2$-digit precision multimeter Keysight 3446A reads out the REF temperature, produced as a calibrated low-voltage signal.

Since, as described, the operating temperature plays a crucial role in the voltage stabilization, being an important parameter in the REFs functioning, the test bench during the measurements is kept inside a custom made *climatic chamber*. The chamber is made by a wooden box, internally coated with aluminum tape acting as a Faraday cage against environmental electromagnetic noise. The temperature is stabilized at approximately room temperature by Peltier cells, providing a total of 250 W of cooling power, with a proportional-integral-derivative (PID) controller, optimized to compensate for the heat produced by the precision multimeters (50 W each) and by the REF chain (about 80 W). The test bench inside the climatic chamber is further placed in a modular container home kept at room temperature by a Mitsubishi air-conditioning unit. After the PID tuning, the temperature inside the climatic chamber can be easily kept constant within a tenth of a Celsius degree, sufficient to avoid strong temperature drift related to the typical seasonal and day-night temperature variations. Finally, the chamber can be flushed with gaseous nitrogen or sulfur hexafluoride to remove humidity and minimize noise from local discharges. The gases have been flushed in many tests showing no relevant improvement on the results, for this reason most of the tests have been conducted in air.

2026 JINST 21 P04009

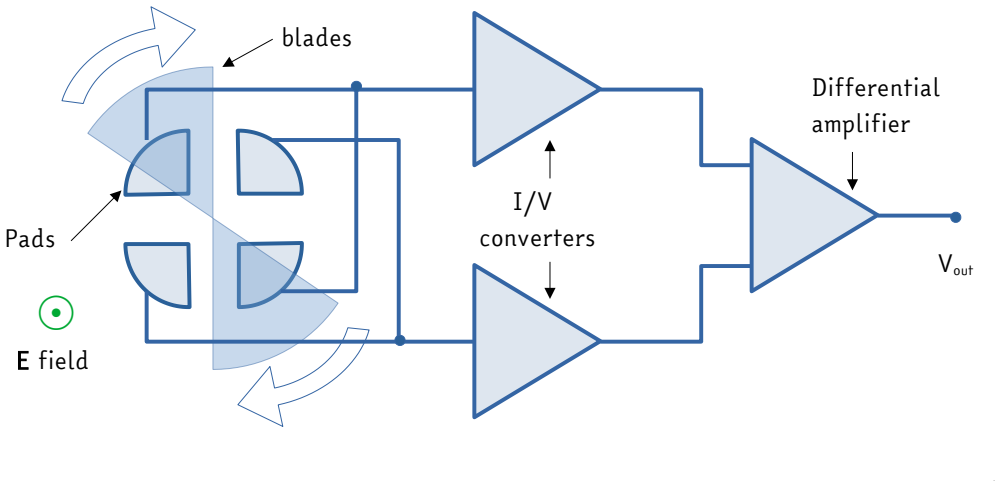

Figure 6. *Field mill* schematic.

A data acquisition (DAQ) system is capable of remotely recording all the digitized precision multimeter signals, along with different probes for monitoring environmental parameters such as temperature in various locations inside the chamber, humidity, and atmospheric pressure. All data, recorded as ASCII files, are catalogued in a database and analyzed by a custom ROOT/C++ based code.

2.1 The *field mill* read-out

A *field mill* is a device used for continuously measuring the strength of electric fields, with many applications in fields such as meteorology, space technology, and other research areas in which continuous and non-invasive electric field measurements are needed [23]. For PTOLEMY, a customized version has been designed and manufactured at the LNGS mechanical workshop.

As shown in figure 6 and the detailed schematic in figure 7, the field mill consists of a top plate connected to the voltage to be measured, separated by a grounded plate through four insulating plastic spacers, shaped to minimize electrical discharges. The central part of the grounded plate, the "mill blade," is shaped like a disk with two trapezoidal holes and rotates about the vertical axis at approximately 3000 RPM (50 Hz) by means of a brushless motor located beneath the plate. Below the mill blade, there are four metallic pads cross-connected in pairs to a low-noise differential amplifier. The pads are electrically isolated from ground by plastic spacers. Due to the spinning blade, the electric field produced by the upper high-voltage plate induces an alternating charge between the two pairs of pads. The resulting amplified signal is approximately sinusoidal with a frequency of 100 Hz (the factor two with the mill speed comes from pads connected in pair at 180°). The signal is then readout by the high precision 8-½ digit "true RMS" voltmeter. The recorded signal is proportional to the electric field produced by the voltage applied to the top plate. Therefore, once the *field mill* output is calibrated, it becomes a high-precision voltmeter.

To guarantee a high level of reliability, the blade spin must be extremely stable. For this reason, a brush-less high-precision motor activated by a driver through a PID controller has been adopted and carefully tuned. Different blade thicknesses have been tested until reaching optimal stability, quantifiable through the fast Fourier transform (FFT) of the output signal. Figure 7 *right* shows an example of comparison between FTTs of the amplifier output signal for two different blade

2026 JINST 21 P04009

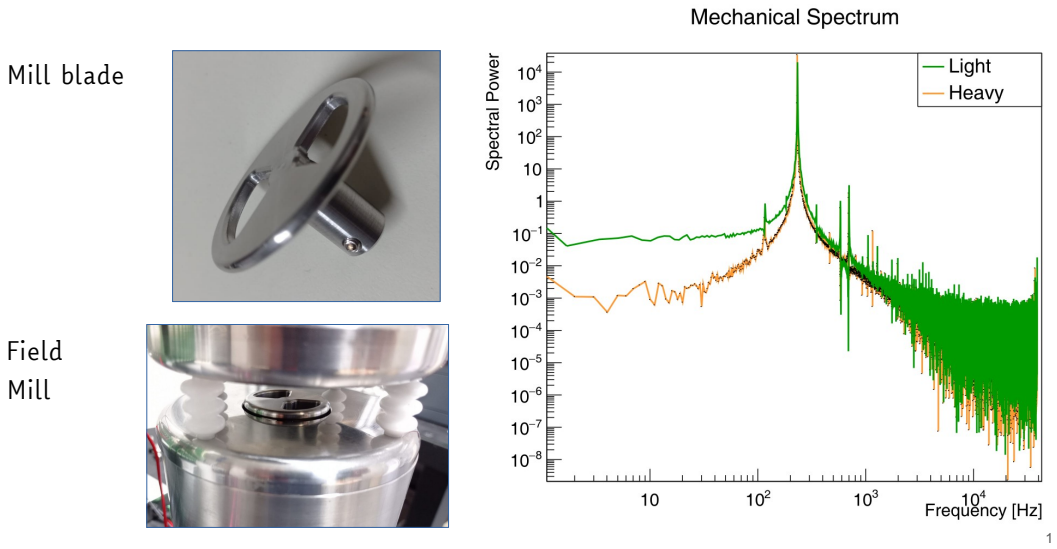

Figure 7. *Left:* picture of the mill blade (*top*) and its position in between the two metal plates (*bottom*). *Right:* comparison between the FFT of two mill blades with different thickness. In this example the heavy version shows a better performance.

thicknesses. Additionally, the motor speed has been optimized to maximize the signal-to-noise ratio, and low-impedance motor grounding has been carefully ensured through full-conductive metal ball bearings lubricated with conductive grease.

Except for the insulating spacers, all the parts of the *field mill* are made from stainless steel. Furthermore, to minimize local electrical discharges, all sharp-edged parts have been properly rounded. In the following section, the first results obtained with the test bench described above are reported.

3 Results

The signal originating from the REF boards typically consists of random Gaussian noise superimposed on long-term variations of the order of tens of minutes, if not hours.

Figure 8 shows an example of recorded data during a 48-hour test. From the *top*, the following measurements are reported: (i) the V_1 voltage from the 500 V pin (half-board) read out by the Keysight $7^1/_2$, (ii) the V_3 voltage from the 1000 V pin (full-board) read out by the Keysight $8^1/_2$, (iii) the internal temperature output voltage V_2 from the first REF in the chain read out by the Keysight $6^1/_2$, and (iv) the temperature (T_1s) in the experimental room (*yellow*) and from the climatic chamber internal sensor (*red*). The last two are measured by commercial sensors read out by an Arduino based system. In general, the trend of the board voltages is characterized by two main time components: a fast decay lasting a couple of hours, and a long-term variation on the order of a few ppm per day, approaching an asymptotic stabilization. The temperature plot shows the accuracy of the thermal stabilization inside the climatic chamber (about 0.1 °C), corresponding to stable environmental conditions in the experimental set-up. Since there is a clear correlation with the board temperature, the fast transient component observed during the first hours is ascribable to

2026 JINST 21 P04009

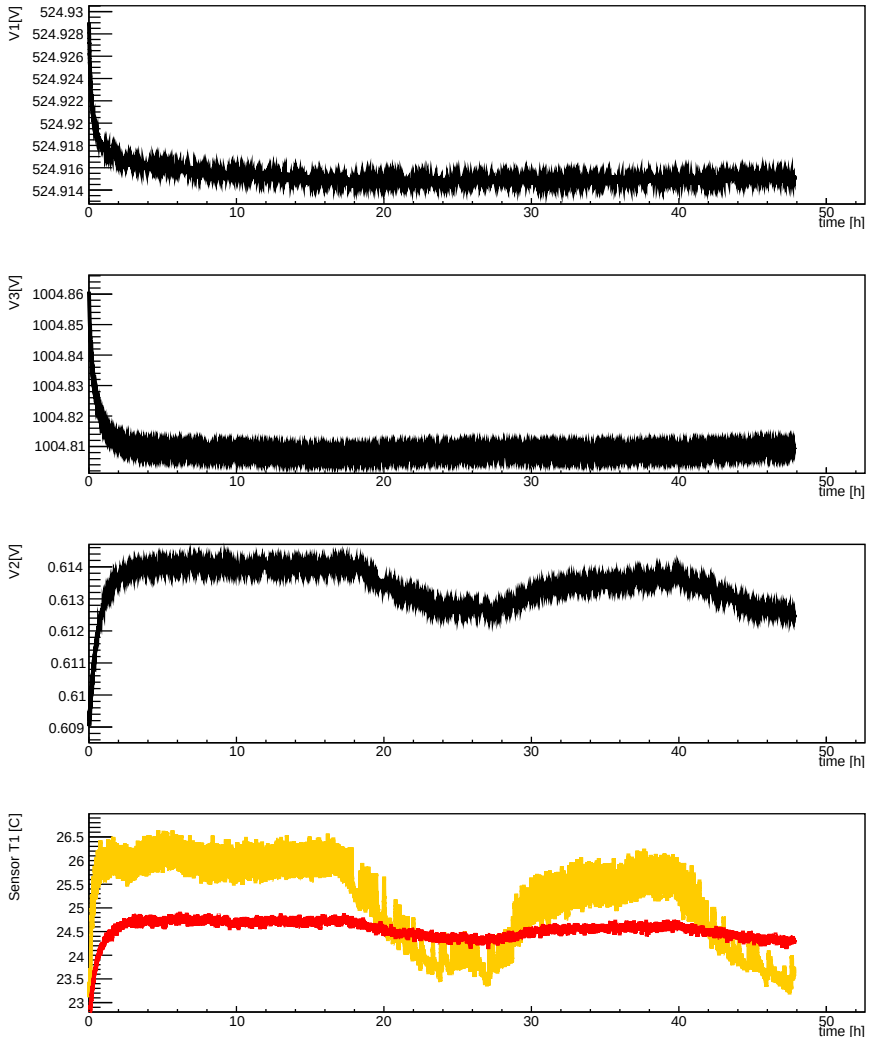

Figure 8. From the *Top*: (i) voltage from 500 V pin (half-board) read out by the KEYSIGHT-7½, (ii) voltage from 1000 V (full-board) read out by the KEYSIGHT-8½, (iii) internal temperature output voltage from the first REF in the chain read out by the KEYSIGHT-6½ and (iv) temperature in the experimental room (*yellow*) and from the climatic chamber internal sensor (*red*).

the thermal stabilization of the board components, which requires some time to take full effect. In general, a sudden change outside the climatic chamber has a non-negligible impact on the Peltier PID control system, as visible in the second half of the time series shown in figure 8. Finally, the residual temperature variations have anyway some direct effect on the board temperature, as evident from the subdominant correlation between T_1 and V_2.

Notice that the total voltage value reads, e.g. 1004 V, which apparently exceeds the accuracy specified by the manufacturer (0.4% instead of 0.05%). The REFs are originally designed to be used as single components and not arranged in a chain with a specific polarization. This non-standard configuration (with a feedback loop) introduces an additional bias in the accuracy; however, it does not affect the overall stability, which is instead improved. As discussed later, this additional uncertainty in the scale can only be removed at the end through the final energy calibration of the filter.

2026 JINST 21 P04009

These long-term variations, often correlated with slow changes in environmental conditions (primarily temperature) or caused by system relaxation, are removed through a *detrending* process. Only the short-timescale voltage fluctuations contribute to the uncertainty in the electron energy measurement. The procedure for removing long-term variations is performed using two different methods. The first method, used for consistency check only, involves fitting the long-term variation to a multi-component exponential curve, which is further corrected with a polynomial depending on the specific case. A second, more flexible, method, used in most of the analysis, consists of a model-independent *detrend* using an optimized first-order local regression (LOESS). The sampled signal $S[n]$ is replaced at each point by the local linear regression:

$$S'[n] = L_k[n, n]\,, \tag{3.1}$$

where $L_k[n, n]$, for each n, is the center of the line $L_k[n, n+m] = \alpha_n(n+m) + \beta_n$ determined using the least squares method within the interval $m \in [-k, +k]$, by minimizing

$$\mathbb{X}^2(\alpha_n, \beta_n) = \sum_{m=-k}^{k} (S[n+m] - L_k[n, n+m])^2\,. \tag{3.2}$$

The parameter k represents the bandwidth of the local smoothing and is determined by minimizing the mean integrated square error over the full time series:

$$\min_k \left\{ \sum_n (S'[n] - L_k[n, n])^2 \right\}\,. \tag{3.3}$$

This optimization ensures that the local regression follows only the long-term trend, leaving the high-frequency random component as a residual:

$$R[n] = S[n] - S'[n]. \tag{3.4}$$

Figure 9 shows an example of REF 1 kV board voltage as a function of time (about 40 h) measured by the $8^1/_2$-digit precision multimeter (*top left*), while the over-imposed *red* curve represents the corresponding LOESS detrend. As visible, the long-term variation occurs over an interval of many hours. The overall variation is about 5 mV, the accuracy of the entire board, made of 100 REFs, is at the level of 5 V, i.e., equal to 0.005% and thus better than the declared technical specification of each single REF (0.025%). This value is compatible with the $\sqrt{100}$ reduction from the independent Gaussian uncertainty propagation, as anticipated in section 2. The precision of the single board, estimated as the RMS of the residues distribution (*bottom left* and *top right*), is in the worst case $\sigma \lesssim 0.2$ mV, corresponding to $\lesssim 0.2$ ppm alone (to be compared with $5 \div 7$ ppm reported in literature [20]). This result is far better than the minimum requirement for the final energy resolution of the PTOLEMY experiment, as described in section 1. Finally the *bottom right* plot reports the discrete fast Fourier transform (DFFT) of the acquired signal, showing no significant periodic component in the time series.

The extrapolation of the precision to the full chain made of 20 boards, read out by the *field mill*, can be described by the following relation

$$\sigma_{20}^2 = \sum_{i,j} \rho_{ij}\sigma_i^2\sigma_j^2 + \sigma_{\text{mill}}^2\,, \tag{3.5}$$

2026 JINST 21 P04009

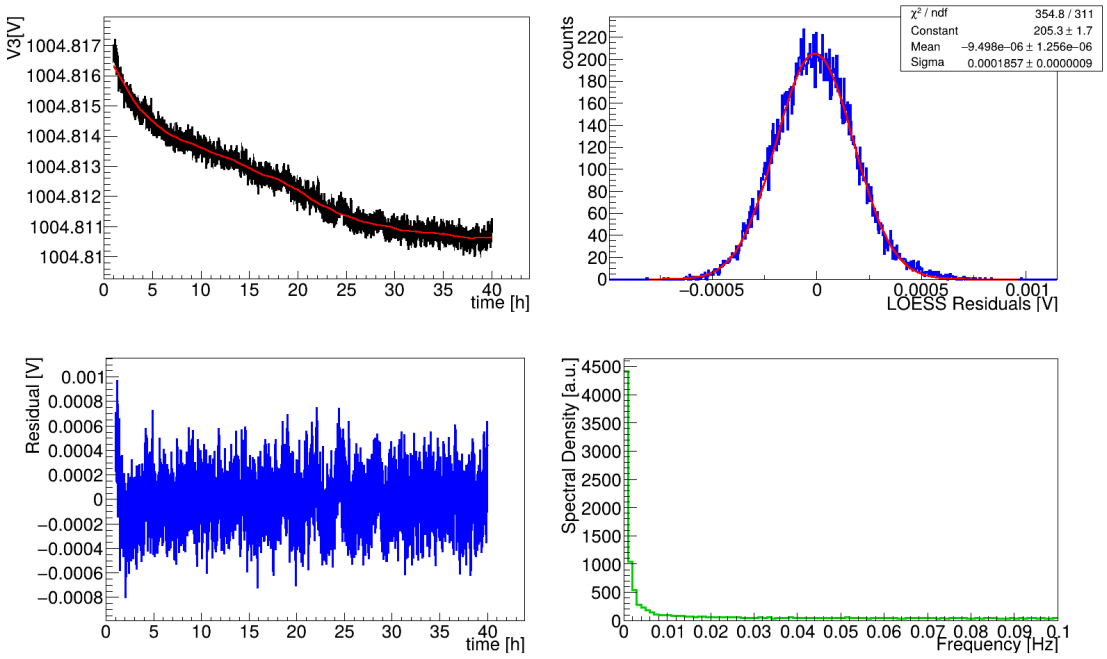

Figure 9. *Top left:* REF board voltage as a function of time measured by the $8^1/_2$-digit precision multimeter. The over-imposed *red* curve represents the local regression. *Top right:* gaussian distribution of the residuals (in *bottom left*) after the LOESS detrend. *Bottom Right:* DFFT of the time series, showing no significant periodic components.

where ρ_{ij} is the correlation matrix describing the extra contribution to the precision coming from possible correlated noise, and σ_{mill} is a possible intrinsic noise contribution due to the *field mill* system. In the most optimistic case, if no extra noise is introduced by the readout device and no correlated noise appears in the full chain, eq. (3.5) becomes the simple sum in quadrature of the single board noise, and the overall precision reads

$$\sigma_{20} = \sqrt{20}\,\sigma_{1\,\text{kV}} \simeq 0.9\,\text{mV}\,, \tag{3.6}$$

resulting in the very small value of $\lesssim 0.05$ ppm, when considered over 20 kV. To evaluate the contribution of the field mill noise, a direct comparison was also performed using a single 1 kV board that was read out simultaneously by precision multimeters and the field mill. However, it was not possible to disentangle the noise contribution, as in the low-field regime the device operates outside its optimal range due to a poor signal-to-noise ratio.

The hypothesis of uncorrelated noise is supported by the comparison of the RMS of the trend of the full board voltage $V_{1\,\text{kV}}$ and the voltage $V_{0.5\,\text{kV}}$ taken from the pin in the middle of the board itself at 0.5 kV. The approximated relation $\sigma_{1\,\text{kV}} \simeq \sqrt{2}\sigma_{0.5\,\text{kV}}$ is basically found, as expected, from the independent uncertainty propagation. Another argument in favor of negligible cross correlation terms arises from the study we performed of possible *phase coherence* and *synchronization* between $V_{1\,\text{kV}}$ and $V_{0.5\,\text{kV}}$. By dividing the time series of the measured voltage residuals $X[i] = V_1(t_i)$ and $Y[i] = V_3(t_i)$, corresponding to the two voltages above, into N_{ck} chunks of 128 sampling points,

2026 JINST 21 P04009

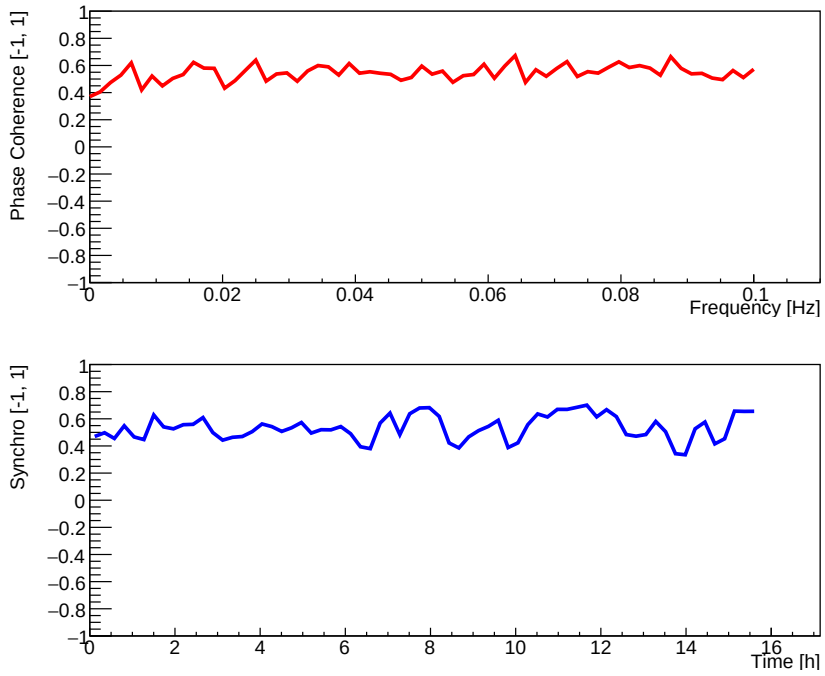

Figure 10. *Top:* phase coherence in chunks of 128 sampling points between $V_{1\,\mathrm{kV}}$ and $V_{0.5\,\mathrm{kV}}$. *Bottom:* synchronization (covariance) between the two measurements in the same chunk. Both plots are calculated in the time interval 3–18 h with high temperature stability.

namely $X_j[i]$ and $Y_j[i]$, the phase coherence for each frequency ω is defined as

$$\gamma(\omega) = \frac{1}{N_{\mathrm{ck}}} \sum_{j=1}^{N_{\mathrm{ck}}} \frac{S_{xy}^{(j)}(\omega)}{S_{xx}^{(j)}(\omega) S_{yy}^{(j)}(\omega)}\,, \tag{3.7}$$

where $S_{xy}^{(j)}$ is the cross-spectral density between $X_j[i]$ and $Y_j[i]$, and $S_{xx}^{(j)}$ and $S_{yy}^{(j)}$ are the (Fourier) spectral densities of $X_j[i]$ and $Y_j[i]$ respectively, done through a DFFT algorithm, respectively. By definition, this quantity ranges in $[-1, 1]$. Alternatively, the synchronization, i.e. the correlation computed chunk by chunk, which also ranges in the same interval, is defined as

$$\rho_j = \frac{\mathrm{Cov}(X_j[i], Y_j[i])}{\sigma_{X_j[i]} \sigma_{Y_j[i]}}\,, \tag{3.8}$$

that is, the covariance between $X_j[i]$ and $Y_j[i]$, normalized to their RMS values.

In figure 10 we report the phase coherence and synchronization between $V_{1\,\mathrm{kV}}$ and $V_{0.5\,\mathrm{kV}}$ over the time interval 3–18 h, corresponding to a highly stable dataset. The plots show a nearly constant value around 0.5 for both $\gamma(\omega)$ and ρ_i, exactly as expected from the number of REFs involved in the overlap (50 out of 100), and without any significant correlation in either phase or time. This supports the optimistic approximation in eq. (3.6).

It is worth pointing out here that precision multimeters cannot measure voltages greater than 1 kV, whereas the 20 kV of the full REF chain can only be monitored by the field mill. In the case of field mill data, however, the situation is a bit worse. In fact, from the measurements conducted

2026 JINST 21 P04009

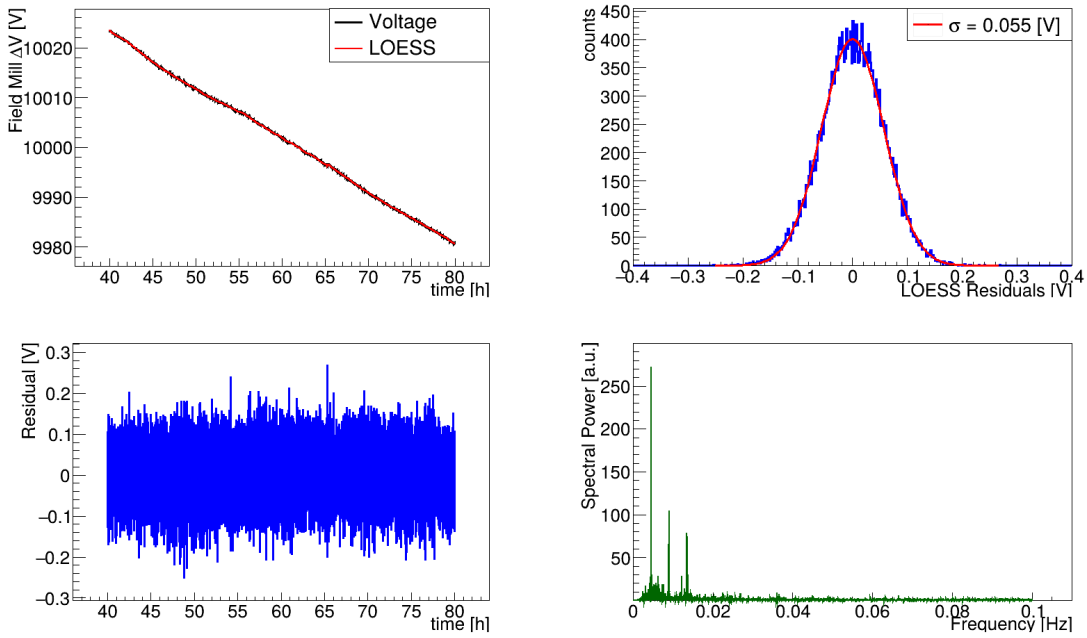

Figure 11. *Top left:* 10-board chain voltage as a function of time measured by the *field mill* device read out by the $7^1/_2$-digit precision multimeter. The over-imposed *red* curve represents the local regression. *Top right:* gaussian distribution of the residuals (in *bottom left*) after LOESS detrend. *Bottom Right:* DFFT of the time series, showing some low frequency periodic component in the time series.

over half the chain (10 boards totaling 10 kV), the precision, as reported in figure 11, is $\sigma_{10} \simeq 50$ mV, corresponding to about 5 ppm, rather than the optimistic ≈ 1 mV coming from the extrapolation in eq. (3.6). Since in the 10-board setup all additional noise sources are already included, it is not entirely incorrect, in this case, to sum in quadrature the precision of the 10-board setup to estimate the precision of the full REF chain. In this less optimistic case, the total precision will be ~ 70 mV, corresponding to ~ 3.5 ppm. In this scenario, the expected contribution to the energy resolution will be, according to eq. (2.1), $\sigma_{\mathrm{HV}}(E) \simeq 70$ meV. This value would be slightly critical for the CνB detection but fully satisfactory for the neutrino mass measurement.

The origin of the extra noise is still under investigation. According to the tests conducted at LNGS, it is unlikely to be due to correlated noise among the boards, as no such correlation is observed when summing every combination of board sub-parts. Instead, it is more likely due to the *field mill* stability and grounding. This explanation is partially supported by the low noise periodic components in the DFFT visible in figure 11 *bottom right*. Furthermore, there was substantial evidence of changes in noise conditions when modifying, e.g., the motor type, the motor driver encoding, the ball bearing resistivity, the mill thickness, and so on.

3.1 Absolute scale calibration

The absolute voltage scale at 10 kV (10 boards), and eventually 20 kV (20 boards), cannot be directly calibrated, as no comparable, independent high-precision reference is available at the moment. It worth reminding that the primary concern is the stability of the reference rather than its absolute accuracy. For the moment, the high voltage in figure 11 is simply extrapolated using the nominal

2026 JINST 21 P04009

value at the end of the chain, according to the simple law

$$V(t) = 10.000 \times \frac{V_{\text{mill}}(t)}{V_{\text{mill}}(0)} \,[\text{V}] \tag{3.9}$$

The final accurate value can only be obtained through a detailed characterization of the individual 1 kV boards forming the full chain and subsequently adjusted in the filter using a calibration source, such as e.g. the monochromatic lines of Kr-83m gaseous low-energy calibration source, anyway both of these procedures go beyond the scope of the present work.

3.2 Fast switch concept

As discussed in section 1, to select electrons with the energy on the region of interest close to the β-spectrum end-point, the electric fields in the novel EM dynamic filter have to be activated on a short time scale of the order of a few milliseconds. This can be realized by a suitable partitioning of the 20 kV REF chain (2000 steps of 10 V each) activated by high-voltage low-noise relays. In order not to disrupt the exceptional stability provided by the REF chain, a careful design is required to maintain, minimize leakage currents, and ensure long-term stability. To achieve this goal, a prototype is being realized at LNGS in cooperation with the electronics laboratory.

It is anyway worth noting that, regardless of the behavior during the transient, the final contribution to the total electron energy due to the electric field is determined solely by V_{in} and V_{out} (basically the potential between the source and the final target), which are highly accurate. Indeed, the "$\mathbf{E} \times \mathbf{B}$" drift in the constant-$B$ field does no work and therefore does not subtract energy from the electrons. Instead, the accuracy of the dynamic voltage only affects the filter efficiency, i.e., the capability of the filter to select a narrow energy region close to the β-spectrum end-point. In practice, this means that the fast-switch transient and its intrinsic roughness do not significantly affect the total contribution to the energy uncertainty, which is ultimately determined by the accuracy of the reference voltage.

4 Conclusions

We have presented, for the first time, the high-voltage (HV) system developed for the electrodes of the PTOLEMY filter. The system, consisting of a chain of 10 V high-precision voltage references arranged in 20 boards of 1 kV read out by a *field mill* device interfaced with precision multimeters, has been demonstrated to achieve an impressive precision of $\sim$ 50 mV over a 10 kV range, which, when extrapolated, translates to an energy resolution contribution of about 70 mV at the tritium end-point (3.5 ppm precision). This level of precision is critical for the detection of CνB, while the current value meets the necessary requirements for a competitive small-scale experiment aimed at measuring the neutrino mass. The time instability of the HV system consists of slow drifts on a time scale longer than the transit time of the electron in the PTOLEMY filter. Those drifts, as shown in section 3, can be easily removed by a *detrend* procedure, and the voltage can be calibrated on the true value via a precision-multimeter in real time.

Considering the intrinsic precision of each 1 kV board (in the worst case 0.2 ppm), there is plenty of room for improvement, up to $\lesssim$ 0.05 ppm from the uncorrelated noise extrapolation. As indicated by different tests, the extra contribution to the noise reducing the performance potentially originates from the mechanical stability, grounding, and the driver of the *field mill* motor plus blade system, while the low-noise amplification system and readout, according to independent measurements, are unlikely to contribute to the reduction in precision.

2026 JINST 21 P04009

Acknowledgments

A. Colijn is supported by the *Dutch Research Council* (NWA.1292.19.231). C. Tully is supported by the *John Templeton Foundation* (No. 62313). This work is also supported by PRIN grant "ANDROMeDa" (PRIN_2020Y2JMP5) of *Ministero dell'Università e della Ricerca*. Finally, the authors acknowledge the support of the INFN CSN-V.

References

[1] J. Lesgourgues, G. Mangano, G. Miele and S. Pastor, *Neutrino Cosmology*, Cambridge University Press (2013) [DOI:10.1017/cbo9781139012874].

[2] PTOLEMY collaboration, *Neutrino physics with the PTOLEMY project: active neutrino properties and the light sterile case*, *JCAP* **07** (2019) 047 [arXiv:1902.05508].

[3] A.G. Cocco, G. Mangano and M. Messina, *Probing low energy neutrino backgrounds with neutrino capture on beta decaying nuclei*, *JCAP* **06** (2007) 015 [hep-ph/0703075].

[4] KATRIN collaboration, *Direct neutrino-mass measurement based on 259 days of KATRIN data*, *Science* **388** (2025) adq9592 [arXiv:2406.13516].

[5] S. Betts et al., *Development of a Relic Neutrino Detection Experiment at PTOLEMY: Princeton Tritium Observatory for Light, Early-Universe, Massive-Neutrino Yield*, in the proceedings of the *Snowmass 2013: Snowmass on the Mississippi*, Minneapolis, MN, U.S.A., July 29–August 6 (2013) [arXiv:1307.4738].

[6] PTOLEMY collaboration, *PTOLEMY: A Proposal for Thermal Relic Detection of Massive Neutrinos and Directional Detection of MeV Dark Matter*, arXiv:1808.01892.

[7] DESI collaboration, *DESI 2024 VI: cosmological constraints from the measurements of baryon acoustic oscillations*, *JCAP* **02** (2025) 021 [arXiv:2404.03002].

[8] https://ptolemy.lngs.infn.it/.

[9] M.G. Betti et al., *Gap Opening in Double-Sided Highly Hydrogenated Free-Standing Graphene*, *Nano Lett.* **22** (2022) 2971.

[10] A. Apponi et al., *Stability of highly hydrogenated monolayer graphene in ultra-high vacuum and in air*, *Appl. Surf. Sci.* **723** (2026) 165658 [arXiv:2504.11853].

[11] Project 8 collaboration, *Tritium Beta Spectrum Measurement and Neutrino Mass Limit from Cyclotron Radiation Emission Spectroscopy*, *Phys. Rev. Lett.* **131** (2023) 102502 [arXiv:2212.05048].

[12] M.G. Betti et al., *A design for an electromagnetic filter for precision energy measurements at the tritium endpoint*, *Prog. Part. Nucl. Phys.* **106** (2019) 120 [arXiv:1810.06703].

[13] A. Apponi et al., *Implementation and optimization of the PTOLEMY transverse drift electromagnetic filter*, 2022 *JINST* **17** P05021 [arXiv:2108.10388].

[14] PTOLEMY collaboration, *A demonstration of slowed electron* $\mathbf{E} \times \mathbf{B}$ *drift for PTOLEMY*, 2025 *JINST* **20** P08025 [arXiv:2503.10025].

[15] PTOLEMY collaboration, *Towards CRES-Based Non-destructive Electron Momentum Estimation for the PTOLEMY Relic Neutrino Detector*, arXiv:2404.00817.

[16] C. Pepe et al., *Detection of low-energy electrons with transition-edge sensors*, *Phys. Rev. Applied* **22** (2024) L041007 [arXiv:2405.19475].

[17] D. Roy and D. Tremblay, *Design of electron spectrometers*, *Rept. Prog. Phys.* **53** (1990) 1621.

2026 JINST 21 P04009

[18] PTOLEMY collaboration, *Heisenberg's uncertainty principle in the PTOLEMY project: A theory update*, *Phys. Rev. D* **106** (2022) 053002 [arXiv:2203.11228].

[19] A. Casale, A. Esposito, G. Menichetti and V. Tozzini, *The β-decay spectrum of Tritiated graphene: combining nuclear quantum mechanics with Density Functional Theory*, arXiv:2504.13259.

[20] A. Smolyakov and M. Gurevich, *Stacking the REF50xx for High-Voltage References*, Application note, https://www.ti.com/lit/an/sbaa203b/sbaa203b.pdf?ts=1747385296724.

[21] T. Thummler, R. Marx and C. Weinheimer, *Precision high voltage divider for the KATRIN experiment*, *New J. Phys.* **11** (2009) 103007 [arXiv:0908.1523].

[22] https://www.ti.com/product/REF50.

[23] https://www.missioninstruments.com/pages/learning/about_fm2.html.

2026 JINST 21 P04009